Effect of the initial spectrum on the spatial evolution of statistics of unidirectional nonlinear random waves

Lev Shemer,[1] Anna Sergeeva,[2] and Dan Liberzon[1]

Received 9 April 2010; revised 11 August 2010; accepted 19 August 2010; published 16 December 2010.

[1] Results of extensive experiments on propagation of unidirectional nonlinear random waves in a large wave tank are presented. The nonlinearity of the wavefield determined by the characteristic wave amplitude and the dominant wave length was retained constant in various series of experimental runs. In each experimental series, initial spectra of different shape and/or width were considered. Every series contained sufficient number of independent realizations to ensure reliable statistics. Evolution of various statistical parameters along the tank was investigated. It is demonstrated that the spectrum width plays an important role in the evolution of the random wavefield and strongly affects the variation of the wave spectrum as well as of parameters that characterize the deviation of the wavefield statistics from that corresponding to the Gaussian distribution. In particular, in a random wavefield that initially contains independent free harmonics within a narrow spectrum, extremely steep waves appear more often in the process of evolutions than predicted by a Rayleigh distribution, while for wider initial wave spectra the probability of those waves decreases sharply and is well below the Rayleigh values.

Citation: Shemer, L., A. Sergeeva, and D. Liberzon (2010), Effect of the initial spectrum on the spatial evolution of statistics of unidirectional nonlinear random waves, *J. Geophys. Res.*, *115*, C12039, doi:10.1029/2010JC006326.

1. Introduction

[2] Ocean waves are both nonlinear and stochastic in nature. While wind serves as a major wave excitation factor, once generated, ocean waves are strongly affected by nonlinear interaction among numerous elementary waves that have random amplitudes and phases. Their evolution in space and time, along with their spectral changes, may be described by advanced deterministic nonlinear equations with random initial conditions. In the process of energy exchange among individual harmonics the energy is transferred to shorter scales, where it is dissipated by breaking or owing to the action of viscosity. A brief review of the theoretical studies dealing with the statistics of random waves was presented in our previous study [*Shemer and Sergeeva*, 2009].

[3] Some measurements of the evolution of unidirectional random wavefields have been performed recently in very large experimental installations. In the experiments of *Onorato et al*. [2005, 2006], the initial Joint North Sea Wave Project (JONSWAP) spectrum was used, with three values of the peak enhancement parameter γ, ranging from 1 to 6, and various significant wave heights for each value of γ. *Shemer and Sergeeva* [2009] studied a unidirectional random wavefield with a much narrower Gaussian-shaped initial spectrum. In their experiments evolution of the wavefield along the tank in multiple realizations of the prescribed initial spectrum was studied for three values of the characteristic wave steepness. These studies provided the experimental evidence that the probability of occurrence of extremely steep (freak) waves may indeed significantly exceed the values corresponding to the Rayleigh distribution. The effect of directional spreading on the statistics of random waves was also considered in a number of numerical and experimental studies [*Socquet-Juglard et al.*, 2005; *Gramstad and Trulsen*, 2007; *Onorato et al.*, 2009; *Waseda et al.*, 2009]. These studies were motivated by the fact that waves in the ocean are indeed nonunidirectional.

[4] The assumption of randomness of the individual harmonics was exploited in numerous attempts to explore the possibility of using deterministic nonlinear wave theories to forecast the evolution of a random wavefield [see, e.g., *Stiassnie and Shemer*, 2005; *Annenkov and Shrira*, 2006; *Onorato et al.*, 2007; *Shemer et al.*, 2010]. In particular, the *Zakharov* [1968] equation was used in numerical simulations by *Stiassnie and Shemer* [2005] and *Annenkov and Shrira* [2006]. The Zakharov equation considers interactions among all possible quartets of waves and thus enables straightforward distinction between those quartets that satisfy exact resonance conditions and those that are only approximately resonant. These theoretical studies demonstrate that near-resonance interactions play a decisive role in the evolution of the statistical characteristics of wavefields owing to nonlinear interactions that occur on the so-called dynamical scale $O(\varepsilon^{-2})$, ε being the characteristic nonlinearity of the wavefield represented by the wave steepness. This is in contrast to

[1]School of Mechanical Engineering, Tel-Aviv University, Tel-Aviv, Israel.
[2]Institute of Applied Physics, Russian Academy of Sciences, Nizhny Novgorod, Russia.

0148-0227/10/2010JC006326

the $O(\varepsilon^{-4})$ scale predicted by the classical kinetic equation of *Hasselmann* [1962], which considers only exact resonances. At a faster evolution scale the exact resonance conditions do not play a decisive role. At this scale the strongest depth of modulation is obtained for near resonance rather than for exact resonance conditions. While detailed discussion of the recent developments in the kinetic wave theory is beyond the scope of this study, two comments may be made here. First, exact resonance conditions cannot be satisfied in a unidirectional wavefield. It may be instructive to recall, therefore, that the most unstable disturbances of a monochromatic wave train due to Benjamin-Feir instability do not satisfy the exact resonance conditions and propagate in the direction of the wave train [see, e.g., *McLean*, 1982]. Second, physical limitations on the size of wave tanks must be dealt with. Evolution on the $O(\varepsilon^{-2})$ scale predicted by stochastic modeling of a nonlinear wavefield can be verified in large wave tanks [see, e.g., *Socquet-Juglard et al.*, 2005; *Shemer et al.*, 2010], whereas any existing experimental facility is too small to enable quantitative verification of the evolution predicted by model computations at slower scales.

[5] Experiments in long wave tanks offer certain advantages over studies in large basins. A large wave tank allows better control of experimental conditions and the possibility of investigating the evolution of the wavefield over considerable distances. In view of the understanding that exact resonance conditions are not exceptionally important in wave evolution at the dynamic scale, experiments in long wave tanks appear to be a suitable vehicle for studying nonlinear random waves under laboratory conditions, complementing measurements in large basins.

[6] While valuable information on the random wavefield statistics was accumulated in the previous investigations of both unidirectional and two-dimensional random wavefields, many questions regarding the evolution along the tank of the statistical wave parameters remain unresolved. In particular, it is unclear whether the spectral shape far away from the wavemaker depends on the initial conditions and whether some equilibrium spectral shape is eventually attained for the given nonlinearity of the wavefield. The relation between the wave height probability distributions, higher moments of the surface elevation, etc., measured far away from the wavemaker, and the initial conditions at the wavemaker is yet to be established.

[7] In the present study the experimental approach of *Shemer and Sergeeva* [2009] is extended and several initial spectral distributions $S(\omega)$ are considered. To separate the effects of nonlinearity and of the spectral shape, an attempt is made to maintain the initial characteristic wave amplitude and frequency constant for each prescribed initial spectrum. Variation of statistical wave parameters along the tank is obtained for a number of initial spectral shapes $S(\omega)$. In particular, the dependence of the probability of appearance of extremely steep (freak) waves is investigated as a function of the initial conditions and of the wavefield evolution stage.

2. Experimental Facility and Procedure

[8] Experiments were carried out in the Large Wave Channel (GWK) in Hannover, Germany, which has a length of 300 m, width of 5 m, and depth of 7 m. The water depth in the present experiments was set to be $h = 5$ m. At the end of the wave tank there is a sloping sand beach starting at the distance of about 250 m from the wavemaker. The computer-controlled piston-type wavemaker is equipped with the reflected wave energy absorption system. The instantaneous water height is measured using 28 wave gauges of the resistance type placed along the tank wall. The closest to the wavemaker gauge was placed at a distance of $x = 3.6$ m from the wavemaker, while the most distant probe was located at $x = 240$ m. The distance between two consecutive probes did not exceed 10 m.

[9] Static calibration of the wave gauges was performed by first filling the tank to a depth of 5.5 m and then reducing the depth to 4.5 m in steps of 0.1 m. The calibration thus covers the range of surface elevations relative to the undisturbed value within ±0.5 m. The linear calibration curve for each wave gauge was obtained by the best-fit procedure. Owing to the size of the facility and the duration of the calibration process, the wave gauges were calibrated only once for each one of the two experimental sessions; each session lasted for about 2 weeks.

[10] To enable direct comparison with *Shemer and Sergeeva* [2009], in all experiments the dominant wave period of $T_0 = 1/f_0 = 1.5$ s was selected, corresponding to a wave length $\lambda_0 = 2\pi/k_0 = 3.51$ m, a dimensionless water depth $k_0 h = 8.95 \gg 1$, and a wave group velocity $c_g = 1.17$ m/s. The deepwater dispersion relation is satisfied for all significant harmonics in the spectrum. Preliminary experiments revealed that the spectra of output signals of the wave gauges exhibit a small but not totally negligible peak at 50 Hz, far beyond the frequency range of interest in this study. Nevertheless, to eliminate possible contamination of the recorded signal by 50 Hz noise due to aliasing, sampling was performed at frequencies ranging from 200 to 300 Hz per channel. Output voltages of all wave gauges, as well as the output of the wavemaker position potentiometer, which provides information on instantaneous wavemaker displacement, were sampled. For reference purposes the wavemaker driving signal was also sampled. The recorded signals were then low pass filtered with a cutoff frequency of 15 Hz, thus effectively eliminating the 50 Hz noise. To avoid storage of unnecessarily long records for further processing, the filtered signal was then digitally "resampled" at the sampling frequency of 40 Hz.

[11] The initial spectra considered differed in both their shape and their width. The dimensionless spectral width ν is defined as

$$\nu = \sqrt{\left(m_0 m_2 / m_1^2\right) - 1}, \tag{1}$$

where the jth spectral moment is defined as

$$m_j = \int_{\omega_{\min}}^{\omega_{\max}} \omega^j S(\omega) d\omega. \tag{2}$$

In equation (2) the integration is carried out over the free wave frequency domain only.

[12] The following initial free wave spectral shapes were considered:

[13] (1) a rectangular spectrum with $f_{\max,\min} = f_0 \pm 0.047$ Hz, $\nu = 0.045$, corresponding to the width of the

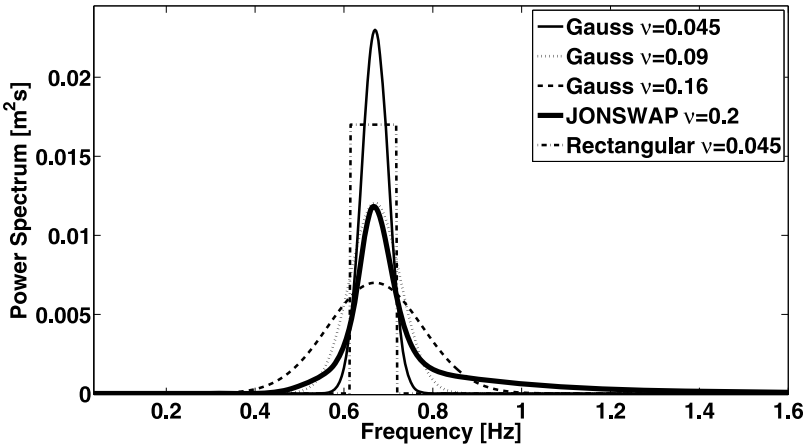

Figure 1. Initial spectral shapes of the surface elevation.

Gaussian spectrum in the experiments reported by *Shemer and Sergeeva* [2009];

[14] (2) a Gaussian spectrum with $\nu = 0.09$;

[15] (3) a Gaussian spectrum with $\nu = 0.16$; and

[16] (4) the JONSWAP spectrum [see, e.g., *Goda*, 2000].

$$S(f) = Af^{-5}\exp\left[-1.25(T_0 f)^{-4}\right]\gamma\exp\left[-(T_0 f - 1)^2/2\mu^2\right]. \quad (3)$$

In equation (3), A is an adjustable amplitude parameter, and the peak enhancement parameter $\gamma = 7$; $\mu = 0.07$ for $f \le f_0$ and $\mu = 0.09$ for $f > f_0$. The dimensionless width of the JONSWAP spectrum with the selected parameters $\nu = 0.20$.

[17] The peak frequency for all spectral shapes was identical to that of *Shemer and Sergeeva* [2009], $f_0 = \omega_0/2\pi = 0.67$ Hz. The spectral amplitudes measured in the vicinity of the wavemaker of each harmonic do not remain fully deterministic owing to the nonlinear response of the water wavefield to the nonmonochromatic wavemaker motion; each of them varies in different realizations of the spectrum around the prescribed value. These amplitudes were also adjusted so that the RMS values of the surface elevation $\sigma = \langle\eta^2\rangle^{1/2}$ in each realization were close to 0.03 m, again as in *Shemer and Sergeeva* [2009], resulting in the nonlinearity parameter $\varepsilon = k_0\sigma \approx 0.054$.

[18] The initial spectral shapes considered in this study are presented in Figure 1. For comparison the narrow Gaussian spectrum considered by *Shemer and Sergeeva* [2009] with $\nu = 0.045$ is also plotted. For each initial shape of the spectrum, the selected duration of the basic unit of the wavemaker driving signal was 81.92 s, corresponding to 4096 data points at a wavemaker driver frequency of 50 Hz and a spectral resolution of the driving signal of 1/81.92 Hz.

[19] To compute the required amplitudes for each spectral harmonic of the wavemaker displacement in every realization of the random wavefield, the linear transfer function for a piston-type wavemaker was applied [*Dean and Dalrymple*, 1991]. In each realization a random phase in the range $[-\pi,\pi]$ was prescribed to each spectral harmonic. The wavemaker driving signal for a given realization was then computed from the resulting complex amplitude spectrum using inverse fast Fourier transform. Frequencies below 0.3 Hz were filtered out from the wavemaker driving signal. No attempt was made to account for free waves at higher harmonics, which are inevitably generated by a piston-shaped wavemaker. The contribution of these waves is relatively minor, both because of their low amplitude and as a result of their propagation velocity, which is substantially lower than that of the dominant wave group. The higher frequency bound waves therefore manifest themselves mainly at record tails that were not considered in the processing and computation of the statistical parameters.

[20] The basic unit of the wavemaker driving signal was repeated twice in each realization, yielding two initially nearly identical wave groups with a signal duration of 163.4 s. This corresponds to about 110 waves at the dominant wave frequency in each realization. About 50 to 70 runs of random-phase realizations for each of the four spectral shapes considered were performed, resulting in a total ensemble of about 5000 to 7500 individual waves for each shape of the initial spectrum.

[21] The first and last values of the wavemaker driving signal, generally speaking, differ from 0. To eliminate large displacements of the wavemaker from its neutral position at the beginning and at the end of the wave excitation period, which can lead to a piston acceleration and velocity beyond the mechanically acceptable limits, signal edge smoothing was used. The driving signal was extended by an additional 8 s. The last 4 s of the basic unit of each realization was added to the beginning of the signal, and the initial 4 s was added to the end of the signal, thus extending the total duration to 171.4 s. The wavemaker driving voltages were then multiplied by the following window function:

$$w(t) = 1 - \exp\left(-\alpha^2 t^2\right), \qquad 0 \le t < 4 \text{ s}, \quad (4a)$$

$$w(t) = \exp\left[-\alpha^2 (t - t_0)^2\right], \qquad 167.4 \text{ s} \le t < 171.4 \text{ s}, \quad (4b)$$

where $\alpha = 1.0\ \text{s}^{-1}$. The total sampling duration was 400 s, to ensure that the whole wavefield excited by the wavemaker propagates beyond the most distant probe within the sampling period. Each consecutive experimental run started only after a sufficient interval from the previous experiment, when the water surface visibly was close to quiescent and

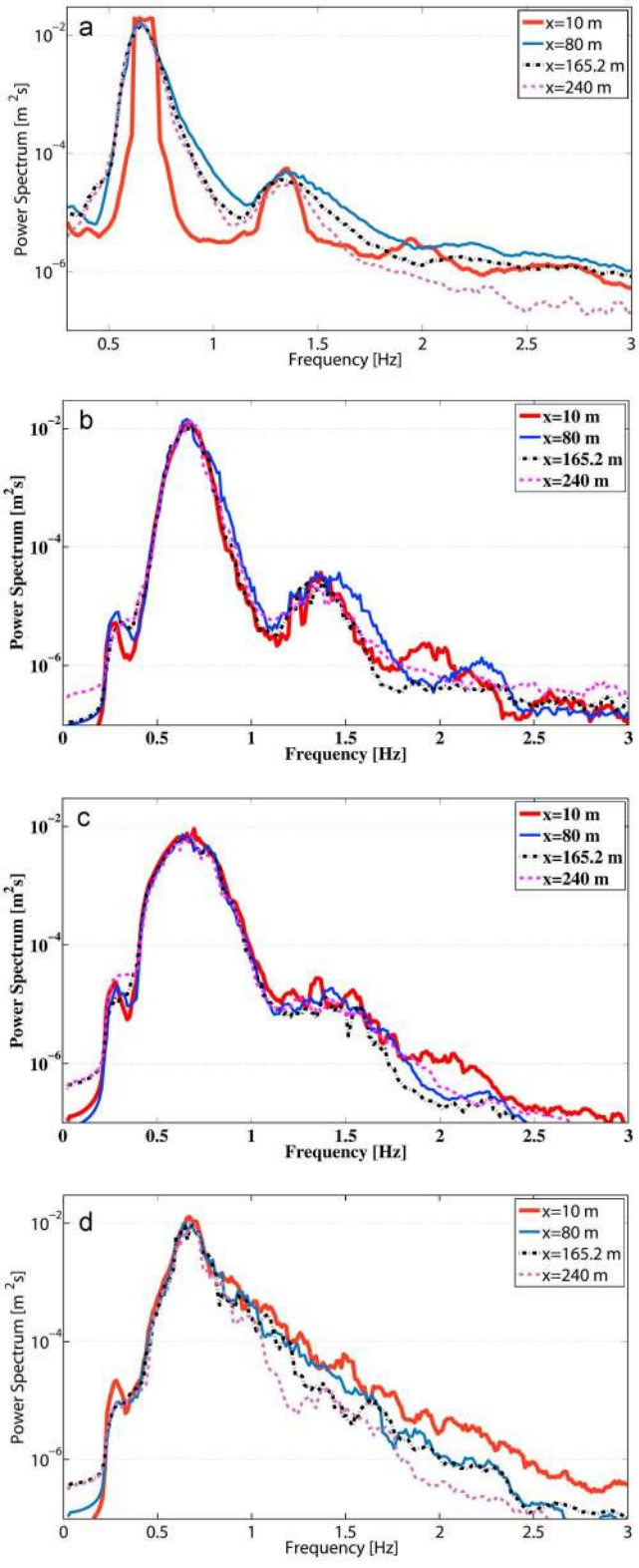

Figure 2. Evolution of the ensemble-averaged wave spectra along the tank: (a) initial rectangular spectrum, $\nu = 0.045$; (b) initial Gaussian spectrum, $\nu = 0.09$; (c) initial Gaussian spectrum, $\nu = 0.16$; (d) initial Joint North Sea Wave Project (JONSWAP) spectrum, $\nu = 0.20$.

remaining disturbances were effectively decayed. The reflected wave energy absorption system eliminated the existing long wave in the tank, which may initially have an amplitude of a few centimeters and is clearly visible to the naked eye; the effective elimination of long waves and relatively fast viscous decay of shorter waves enabled quite short (about 10 min) intervals between experimental runs.

3. Results and Discussion

[22] The measured evolution along the tank of wave spectra with different initial spectral shapes is illustrated in Figure 2. For all initial spectra considered the results are shown at four locations along the tank, up to x = 240 m, where the most distant wave gauge was located. The actual initial conditions in experiments can be estimated from data obtained by the wave gauge at x = 10 m, which is close to the wavemaker but beyond the domain where a significant contribution of evanescent modes can be expected [*Dean and Dalrymple*, 1991]. Figure 2 demonstrates that at this location, in each case the prescribed spectral shapes are indeed reproduced reasonably well in the experiments. For all cases presented in Figures 2a–2d, the peak frequency does not change notably along the tank. Considerable variation in the spectral shape at a distance x from the wavemaker is obtained mainly for the initially rectangular narrow spectrum in Figure 2a. This spectrum does not retain its rectangular shape and becomes substantially wider at x = 80 m; the spectrum then becomes narrower again. Note that at x = 80 m, only the part of the spectrum at frequencies exceeding the peak value differs notably from that at more distant locations, whereas the low-frequency part of the spectrum does not change significantly after a few tens of dominant wave lengths λ_0. The effect of widening of the higher frequency part of the spectrum at x = 80 m is also distinguished in Figure 2b. For the even wider initial spectral shapes in Figures 2c and 2d, no such widening is obtained. The spectra in Figure 2c do not exhibit any significant modification along the whole tank. Note that the results in Figures 2a and 2b demonstrate that equilibrium spectral shapes are attained in those cases at distances exceeding about $40\lambda_0$. Those equilibrium shapes, however, are not universal and are strongly dependent on the initial spectrum.

[23] For the initial JONSWAP spectral shape (Figure 2d), the high-frequency part of the spectrum seems to decay monotonically, and the total power decreases along the tank. It should be noted in this respect that despite the fact that, for all spectral shapes considered, the initial wave steepness $\varepsilon = k_0\sigma$ was maintained approximately constant, sporadic wave breaking at various locations along the tank was observed for the JONSWAP initial spectrum, while for the other spectral shapes virtually no breaking could be detected visually. The wave energy decay in Figure 2d is apparently related to this occasional wave breaking.

[24] Spectral moments computed over free waves only are required to determine the spectral width according to equations (1) and (2). It is clearly shown in Figures 2a and 2d that the separation of domains of free and second-order bound waves changes significantly with the initial spectral width. For narrow spectra the frequency domains corresponding to free and bound waves are clearly separated (Figure 2a [see also *Shemer and Sergeeva*, 2009]), thus

making the distinction between these waves relatively simple. The domains around the dominant frequency and its second bound harmonic are still somewhat separated in the case of the wider spectrum in Figure 2b. For even wider spectra, however, the free and the bound waves may have overlapping frequency domains, and the separation between them requires more attention. To extract free wavefields from the wave records that apparently contain bound as well as free waves, an iterative procedure based on the *Zakharov* [1968] equation and related expressions for bound waves given in the Appendix of *Stiassnie and Shemer* [1987] was used. The algorithm was originally derived for deterministic wavefields with a wide spectrum by *Shemer et al.* [2007] and allows accounting for bound waves up to the third order. However, the third-order bound waves have very low amplitudes that are comparable with the experimental inaccuracy. Taking into account also the substantial computer resources required for computation of those waves for the large number of realizations recorded in the present study, only bound waves of the second order are considered here.

[25] For each realization of the prescribed initial spectrum and for each wave gauge, the wave-containing part of the record was divided into 20 s long segments (with 50% overlap between the consecutive segments), and separation of free and bound waves was performed for each such segment. Following *Shemer et al.* [2007], we start with the measured temporal variation of the surface elevation as the initial guess for the free wavefield. The computed second order bound waves corresponding to this free wavefield are then subtracted from the full record, and the result serves as the next approximation of the free wave field. The process converges after a few iterations. A different method to account for bound waves was suggested by *Fedele et al*. [2010]. Their approach, while somewhat faster, is based on the nonlinear Schrödinger equation and is therefore less suited for wider spectra.

[26] The wave spectra corresponding to the free and the second order bound waves were calculated for each segment and then averaged over all segments of all realizations for each gauge separately. The variation along the tank of the resulting free and bound wave spectra for the widest initial Gaussian-shaped spectrum is presented in Figure 3. Despite the fact that the initial spectrum is relatively wide, the frequency domains of the free and the second-order bound waves appear to be separated. Note also that, as expected, the bound wave spectrum is wider than that of the free waves but shows much lower amplitudes. Two domains of bound waves are clearly visible in Figure 3b: a domain of bound waves having frequencies that correspond to the summation of the generating free wave frequencies, centered in the vicinity of the second harmonic of the dominant free wave; and a domain of bound waves at low frequencies that corresponds to the free wave frequency difference.

[27] To examine the efficiency of separation of the free and bound parts of the wavefield, the third-order moment of the surface elevation, the so-called skewness coefficient, defined as

$$\lambda_3 = \langle \eta^3 \rangle / \sigma^3, \tag{5}$$

was calculated. The values of λ_3 are plotted in Figure 4 for two cases with an initially Gaussian spectral shape and different widths, $\nu = 0.09$ and $\nu = 0.16$. In both cases the skewness of the free wavefield remains very small along the whole tank, as expected. The vanishingly small values of λ_3 corresponding to the computed free wavefield serve as an indication that the separation between free and bound waves was performed properly.

[28] Contrary to the free wavefield, the full wavefield exhibits significant positive values of λ_3 that are quite similar for both initial spectral widths along the whole tank, being mostly somewhat below $\lambda_3 = 0.2$. These positive values of λ_3 result from the crest-trough asymmetry of nonlinear waves, which apparently is sensitive primarily to the nonlinearity, which is very similar in both Figure 4a and Figure 4b. The only significant differences between Figure 4a and Figure 4b occurs for an initially narrower spectrum, where at about $x = 70$ m the values of λ_3 grow notably, to attain a maximum that exceeds 0.2. This variation of the skewness coefficient with the distance x in Figure 4a is qualitatively similar to that reported by *Shemer and Sergeeva* [2009] for an initially narrower Gaussian spectrum.

[29] The variation along the tank of the spectral width ν computed according to equations (1) and (2), with integration in equation (2) carried out for the free wavefield only, is presented in Figure 5. The variation of the spectral width ν measured in the present experiments is compared in Figure 5 with that reported by *Shemer and Sergeeva* [2009] for a narrow initial Gaussian spectrum at the same experimental facility. It appears that the variation of ν with the distance x from the wavemaker is virtually identical for both Gaussian and rectangular spectra with the initial value of $\nu = 0.045$. For this initially very narrow spectrum the number of discrete free harmonics in the initial wavemaker driving signal is quite small, less than 10 in both studies. The actual difference between the initial spectra in these studies is not very significant, and in fact after about 50 m (no wave gauges closer to the wavemaker were available in the older experiments that were carried out in 2003), the ensemble averaged spectra become essentially identical. There is a 6 year time gap between the experiments with the narrow Gaussian spectra and those in the present study, as well as numerous differences in the methodology of the experiments. Nevertheless, excellent quantitative agreement is obtained between the two totally different experimental sessions, demonstrating a high repeatability and accuracy of the results.

[30] The results presented in Figure 5 are for all wave gauges employed and corroborate the result shown in Figure 2, that the evolution of the spectral width along the tank is strongly dependent on the initial values of ν. For initially wider spectra the variation of ν along the tank becomes less pronounced. For all Gaussian shapes considered, as well as for the initially rectangular free wave spectrum, the spectral width seems to attain a quasi-equilibrium value at distances exceeding about 170 m (about 50 dominant wave lengths) from the wavemaker. These quasi-equilibrium spectral widths are different for all spectral shapes considered. For initially very narrow spectra with $\nu = 0.045$, the quasi-equilibrium width corresponds to about $\nu \approx 0.08$, while for the initially widest Gaussian spectral shape employed in the present experiments, as well as for the JONSWAP spectrum, the far-field value of ν is nearly twice as large, reaching $\nu \approx 0.15$.

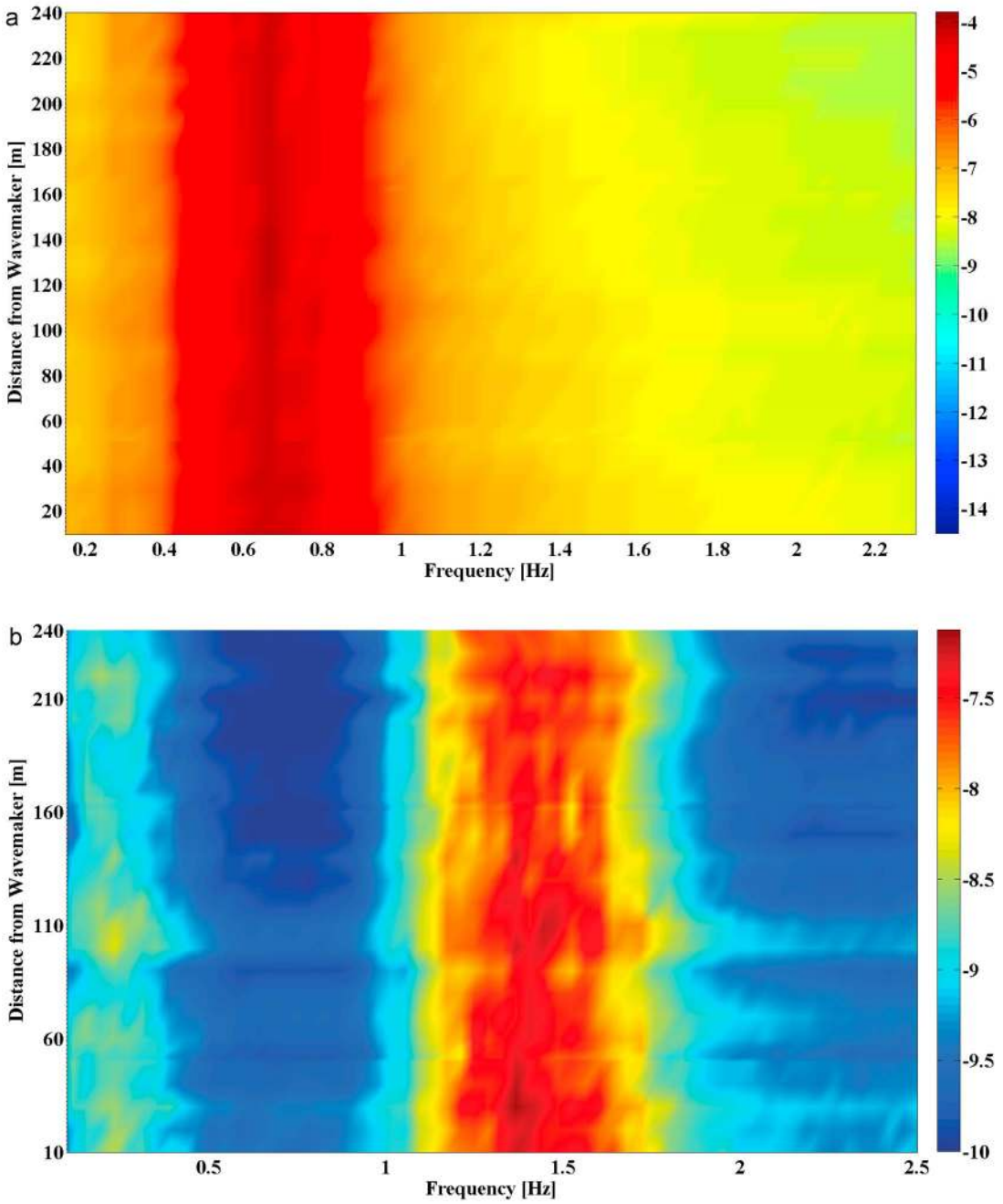

Figure 3. Variation of the power spectra (as a color map; m^2/Hz, logarithmic scale) along the tank for the initial Gaussian spectrum with $\nu = 0.16$: (a) free waves; (b) second-order bound waves.

[31] The evolution of the spectral width of a random wavefield with the initial spectral shape given by equation (3) (JONSWAP spectrum) is somewhat different from that observed for other initial conditions. The initial width of this spectrum exceeds that of other spectral shapes considered. The values of ν in Figure 5d tend to decrease along the tank, so that at $x > 200$ m the spectral width in this series of experiments falls below the values of ν that correspond to an initially narrower Gaussian spectrum. The decrease in spectral width with distance seems to be closely related to decay in the total wave energy and thus to the level of nonlinearity along the tank as discussed with relation to Figure 2d.

[32] The deviation of the wavefield statistics from Gaussianity can be characterized by the fourth momentum, the kurtosis λ_4:

$$\lambda_4 = \langle \eta^4 \rangle / \sigma^4. \tag{6}$$

For a Gaussian wavefield, $\lambda_4 = 3$. The variation of λ_4 with the distance x is plotted in Figure 6 for two Gaussian-shaped initial spectrum with the width v = 0.16.

[33] Two conclusions can be drawn from Figure 6. The first is that the kurtosis values calculated for the random

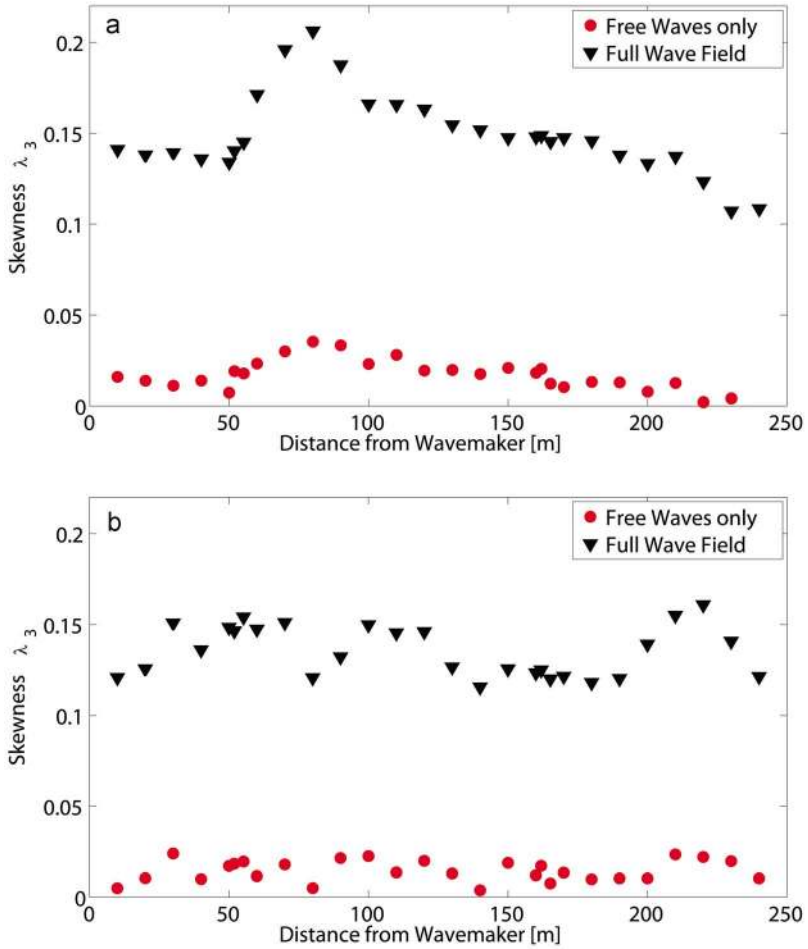

Figure 4. Variation along the tank of the skewness λ_3 for initial spectra with a Gaussian shape: (a) $\nu = 0.09$; (b) $\nu = 0.16$.

wavefield that contains only free waves do not differ significantly from $\lambda_4(x)$ based on the full wave records. The contribution of second-order bound waves to λ_4, although apparently always positive, appears to be insignificant. This result is in general agreement with *Shemer et al.* [2010], where the numerical simulations based on the experimental data of *Shemer and Sergeeva* [2009] demonstrated that, for a narrow initial spectrum, the contribution of bound waves to kurtosis, while somewhat more pronounced than in the present experiments with wider initial spectra, remains of

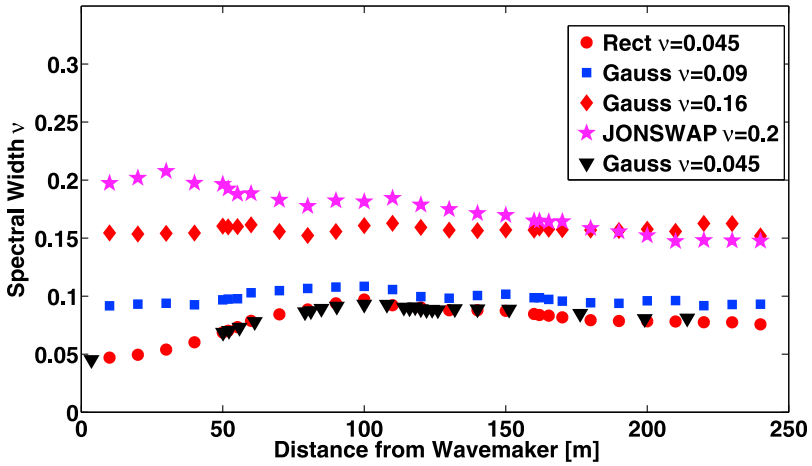

Figure 5. Spectral width ν as a function of distance from the wavemaker for different initial spectral shapes.

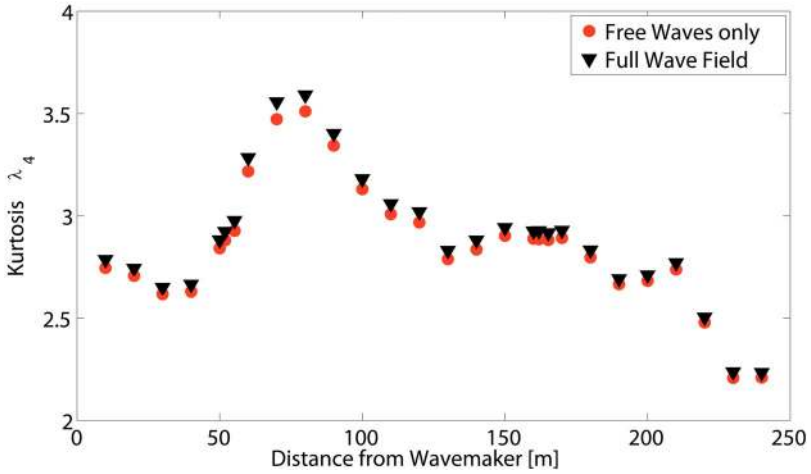

Figure 6. Variation of full and dynamic (for free waves only) kurtosis along the tank for an initial Gaussian spectrum, $\nu = 0.16$.

minor importance. These observations differ somewhat from the numerical results of *Annenkov and Shrira* [2009], who carried out Monte Carlo simulations of the temporal evolution of an initially unidirectional wavefield using the *Zakharov* [1968] equation. The simulations by Annenkov and Shrira were performed for a spectral width similar to that in Figure 6b, but for a higher nonlinearity of the wavefield. Their numerical results indicate that while the portion of kurtosis owing to free waves only (dubbed in this study the "dynamic" kurtosis) is indeed dominant in the determination of the total value of λ_4, the contribution of bound waves nevertheless remains important.

[34] The second conclusion that can be drawn from Figure 6 is related to the kurtosis values. The variation of kurtosis along the tank presented in Figure 6 exhibits both similarities to and differences from the results of previous studies. In agreement with both *Shemer and Sergeeva* [2009] and *Annenkov and Shrira* [2009], during the initial stages of evolution, up to about 70 m (or 20 dominant wave lengths) the values of kurtosis increase sharply, then decrease farther away from the wavemaker, exhibiting some oscillations. It should be stressed, however, that the deviations of λ_4 from the value of 3 that corresponds to the Gaussian distribution are relatively modest and, in most cases, do not exceed 0.5. This is in contrast with the results of Shemer and Sergeeva and of Annenkov and Shrira, where the excursions of λ_4 from the value that corresponds to the Gaussian distribution were much more significant. It is also worth noting that, starting from about $x = 120$ m, the kurtosis assumes values that are mostly below $\lambda_4 = 3$, thus indicating that deviations from Gaussianity for wider spectra are qualitatively different from those observed for a narrow initial spectrum.

[35] The experimentally determined wave height distributions $F(H)$, normalized by the RMS values of the surface elevation σ, are presented in Figure 7 for an initially Gaussian spectrum with $\nu = 0.16$ at six selected distances from the wavemaker. The experimental results are compared in Figure 7 with the Rayleigh distribution, as well as with the distribution developed by *Tayfun and Fedele* [2007], which accounts for the nonlinearities of the third order. The theoretical distributions were calculated using equations (41), (58), and (62) in that paper for wave height, crest, and trough, respectively, while the parameters characterizing the fourth-order cumulants and the wave steepness were determined according to equations (42) and (56). In Figure 7 the experimental curves do not differ significantly from the Rayleigh distribution, as long as the wave heights do not exceed about 4σ, although even for those wave heights some deviations from the Rayleigh distribution are observed, most prominently at $x = 80$, 150, and 220 m. For higher values of H/σ, deviation of the wave height probability distributions from the Rayleigh shape occurs in both directions. These deviations from the Rayleigh distribution are closely related to the local value of λ_4; the measured probability distribution exceeds the Rayleigh values when the local kurtosis is >3 and falls below the corresponding Rayleigh values for $\lambda_4 < 3$. Oscillations of the distribution tails are predicted reasonably well by the Tayfun and Fedele distribution. It should be stressed, however, that the theoretical distribution in most cases seems to overpredict the probability of appearance of the steepest waves in the ensemble.

[36] A prominent feature of the distributions plotted in Figure 7 is the virtual absence in the accumulated ensemble of waves with heights exceeding 8σ, which can be considered "freak" waves. This result is quite different from the distributions presented by *Shemer and Sergeeva* [2009] for a narrow Gaussian-shaped initial spectrum ($\nu = 0.045$), where the probability of extremely high waves was significantly higher than that corresponding to the Rayleigh distribution. Moreover, in the measured distributions presented in Figure 7 the tail of the distribution that corresponds to the steepest waves in the ensemble turns sharply down. This part of the distribution is in most cases not presented adequately by the Tayfun-Fedele curves.

[37] The corresponding distributions for wave crests and troughs are presented in Figures 8 and 9, respectively. Owing to the wave asymmetry the crest heights attain higher values than the troughs. Both crest and trough distributions at normalized values exceeding about 2 oscillate around the Rayleigh curve. It appears that the Tayfun distributions in Figures 8 and 9 perform somewhat better than that in Figure 7 for representing the most extreme waves in the ensemble.

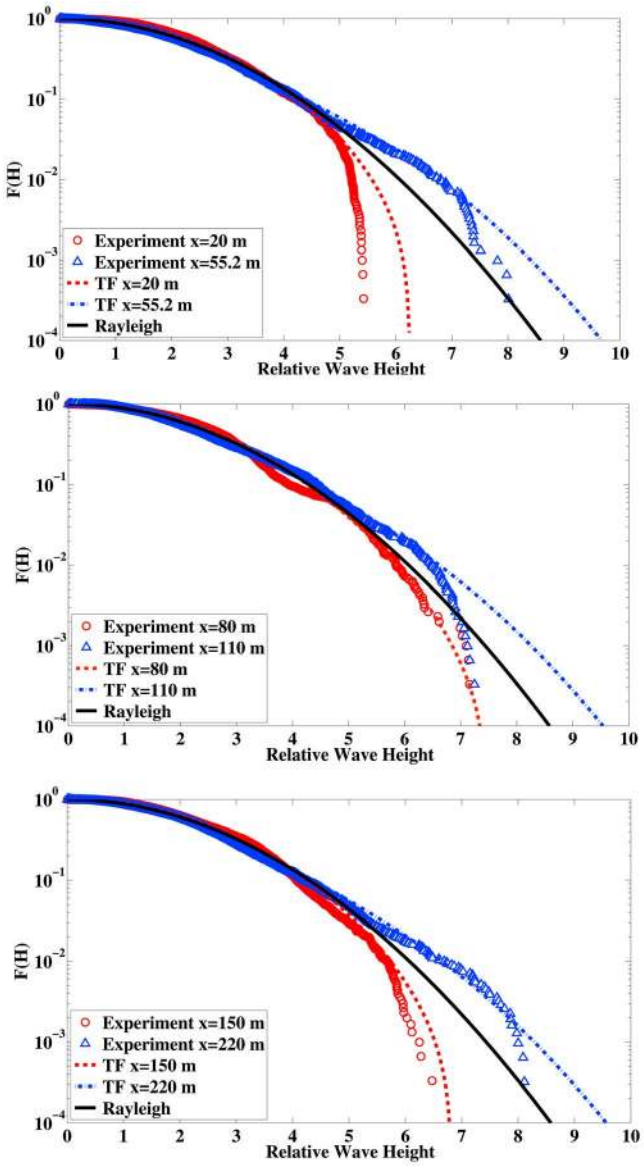

Figure 7. Comparison of experimentally determined wave height probability distributions with the Rayleigh and the third-order Tayfun-Fedele distributions at various locations along the tank for an initially Gaussian spectrum with ν = 0.16. Wave heights are normalized by the RMS values of the surface elevation σ.

[38] The relation between the local value of the kurtosis and the probability of appearance of relatively high waves is further studied in Figure 10 for three initial spectral shapes: a rectangular spectrum (ν = 0.045), a Gaussian spectrum with ν = 0.09, and the JONSWAP spectrum with ν = 0.20. In each of the three cases considered the variation along the tank of the probability of appearance of waves exceeding three prescribed values H^* is presented; to examine the deviations from Gaussianity, the experimentally determined probability for each H^* is normalized by the corresponding value obtained from the Rayleigh distribution. These probabilities are juxtaposed on the same plot with the variation of kurtosis with distance from the wavemaker.

[39] The kurtosis variation presented in Figure 10 is discussed first. The values of the kurtosis are notably different in Figures 10a, 10b, and 10c. In the initially narrow rectangular spectrum case (Figure 10a), λ_4 is somewhat below 3 close to the wavemaker but increases rapidly to very high values, attaining a maximum of about λ_4 = 6 at approximately 100 m (30 dominant wave lengths λ_0) from the wavemaker. Farther away the values of λ_4 decrease but remain well above λ_4 = 3 for the whole length of the tank. The values of kurtosis in Figure 10a are thus notably higher than those obtained for the wider initial spectrum in Figure 6, as well as in Figures 10b and 10c. These results in Figure 10a are, however, in excellent agreement with the variation of $\lambda_4(x)$ reported by *Shemer and Sergeeva* [2009] for a initially very narrow Gaussian spectrum with an initial width as in Figure 10a.

[40] The dependence $\lambda_4(x)$ in Figure 10b for a Gaussian spectrum with ν = 0.09 is qualitatively similar to that shown

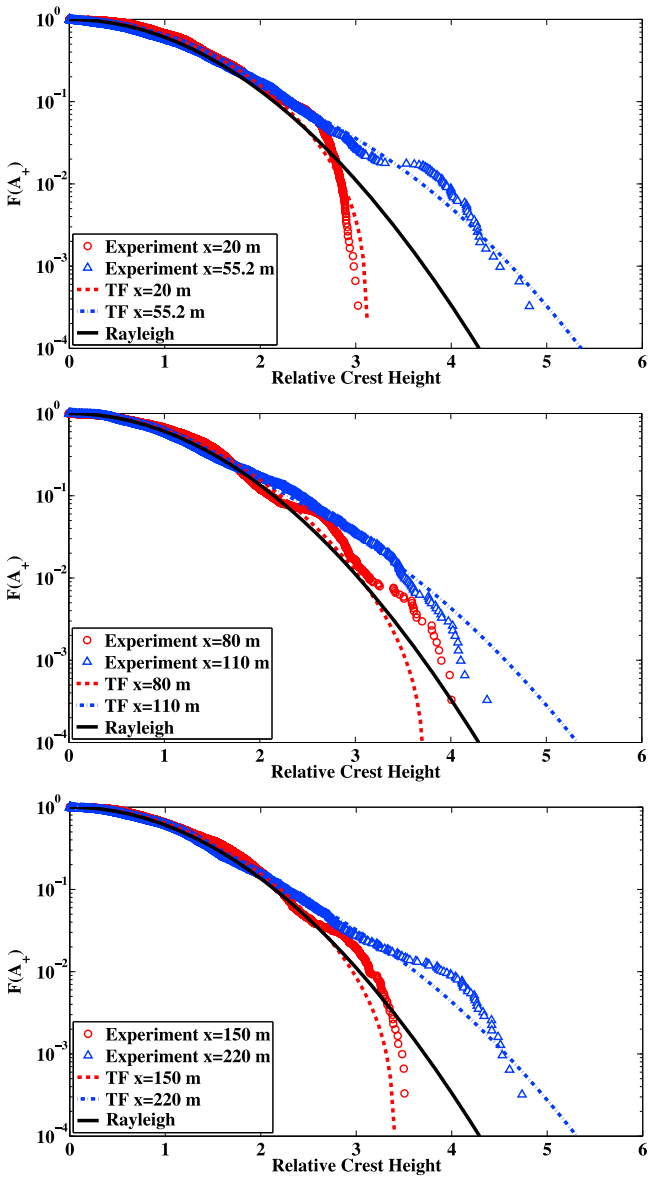

Figure 8. As Figure 7, for wave crests.

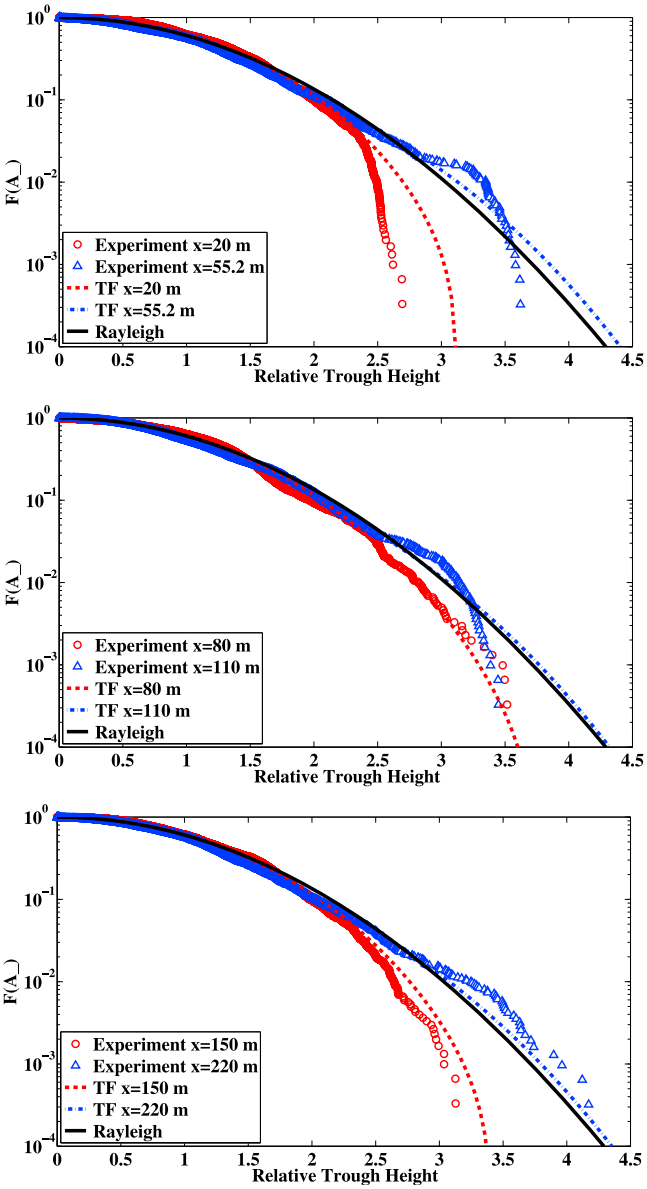

Figure 9. As Figure 7, for wave troughs.

in Figure 10a, growing initially and attaining a maximum at about 75 m ($20\lambda_0$); the subsequent decrease in λ_4 with the distance is close to monotonous. Quantitatively, the values of kurtosis in Figure 10b, however, are well below those in Figure 10a and are closer to those in Figure 6 for the wider Gaussian spectrum with $\nu = 0.16$, although they are generally somewhat higher. For the initially wider JONSWAP spectrum, the values of λ_4 do not differ significantly from those in Figure 6; they vary slightly along the tank and somewhat exceed the value of 3 up to about 180 m from the wavemaker, falling below $\lambda_4 = 3$ farther away. This decrease in λ_4 may be related to wave breaking that was observed for the experiments with the JONSWAP spectrum as already discussed.

[41] Much higher waves were observed for the initial rectangular narrow spectrum than for all other cases with higher initial values of ν. The wave heights H^* selected for comparison represent the relatively steep waves in the ensemble for which sufficient statistics still exists. Much higher waves were observed for the initial rectangular spectral shape, hence, the selected values of H^* in Figure 10a are above the generally accepted freak wave limit. The relative probability of these waves increases with H^*, and for $H^*/\sigma = 9.5$ it attains values that are higher than the Rayleigh-distribution-based prediction by a factor that exceeds 400. Probabilities significantly higher than those corresponding to the Rayleigh distribution were also obtained for somewhat smaller waves. The deviations from the Rayleigh distribution in Figure 10a closely follow the variation in the kurtosis along the tank and attain a maximum in the vicinity of the maximum of $\lambda_4(x)$.

[42] For wider initial spectra (Figures 10b and 10c), extremely high waves were not observed (cf. Figure 7). The comparison is thus carried out for waves that, while exceeding the significant wave height, are well below the freak wave definition. The deviations from the Rayleigh distribution for these waves in both Figure 10b and Figure 10c are much less dramatic than those in Figure 10a. In Figure 10b the probability of these waves is higher than that given by the Rayleigh distribution by a factor that usually does not exceed about 2.5. The variation of the deviation from the Rayleigh distribution along the tank closely follows the dependence $\lambda_4(x)$. At a location with $\lambda_4 < 3$, the probability of the relatively high waves considered in Figure 10b is lower than that given by the Rayleigh distribution.

[43] For the JONSWAP spectrum (Figure 10c), the wave probabilities generally differ from the Rayleigh prediction by a factor that does not exceed 2. Although the pattern of wave height probability variation with x is less organized in Figure 10c, the close relation between the deviations from the Rayleigh distribution and the local value of λ_4 can be discerned in this figure as well. At large distances from the wavemaker, $x > 180$ m, the probability of relatively high waves falls below the Rayleigh value, in agreement with the strong decrease in kurtosis at these locations.

[44] The results in Figure 10 thus demonstrate that the highest waves are mostly associated with initial free wave spectra that are narrow and consist of harmonics with uncorrelated and uniformly distributed phases. These findings may be related to the observations by *Gramstad and Trulsen* [2007] and *Onorato et al.* [2009] that both the probability of appearance of extreme waves and the kurtosis decrease as the directional spreading becomes wider. In those studies the probabilities of very steep waves are mostly higher than those corresponding to the Rayleigh distribution, and the values of kurtosis usually exceed 3. In some cases with wide directional spreading, however, *Onorato et al.* [2009] obtained probabilities of extreme waves that fall below the Rayleigh predictions in their experiments. As the directional spreading increases, wave spectra consist of a larger number of free harmonics. The relatively low probability of very steep waves thus seems to be related to the number of free harmonics in the spectrum, both in unidirectional and two-dimensional wavefields.

[45] Extremely high waves thus tend to appear more often than predicted by the Rayleigh distribution only for initially narrow spectra. The probability of these waves, however, attains a maximum when the initial spectrum reaches its highest possible width [see also *Shemer and Sergeeva*, 2009]. An example of a single realization of an initially

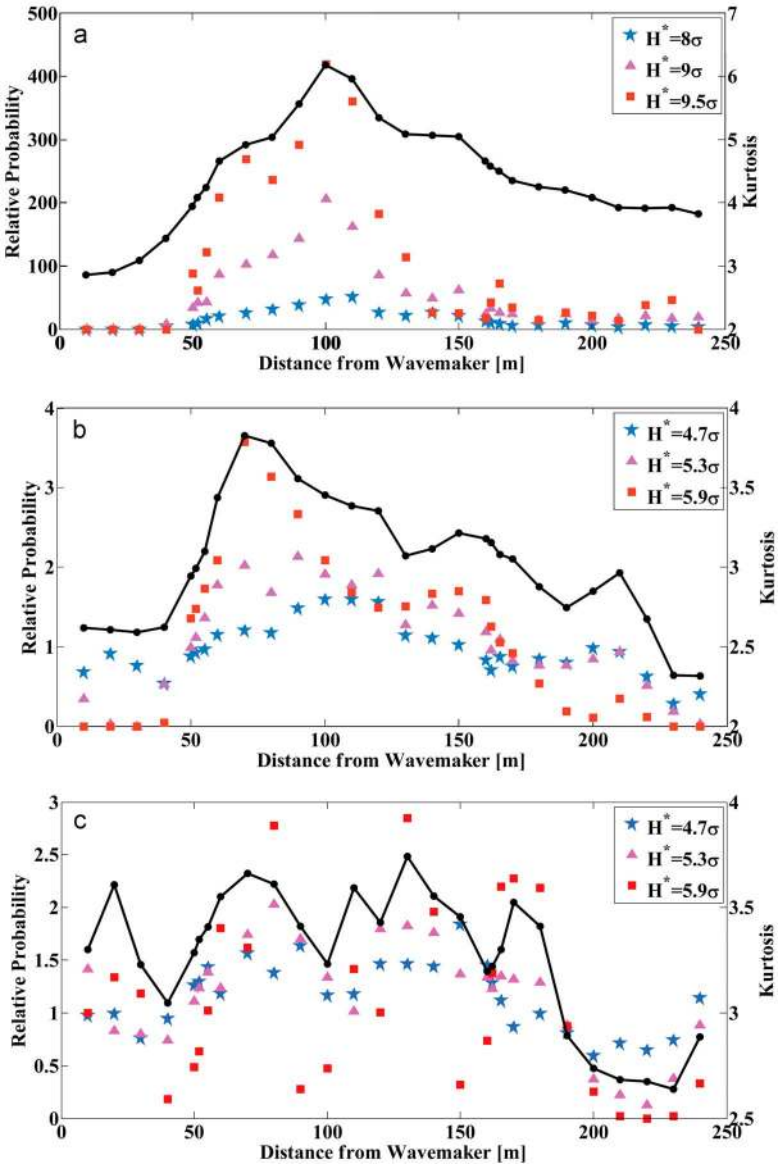

Figure 10. Comparison of the probability of the highest waves in the ensemble relative to the Rayleigh distribution, $F(H > H^*)/F_R(H > H^*)$ (left vertical axis), and the kurtosis (right vertical axis) as a function of the distance from the wavemaker: (a) rectangular initial spectrum, $\nu = 0.16$; (b) Gaussian initial spectrum, $\nu = 0.09$; (c) JONSWAP initial spectrum, $\nu = 0.20$.

rectangular spectrum where extremely high waves were measured is presented in Figure 11. Two nearly identical wave groups are visible in this record; in each group a very steep wave was observed, with the height of the highest wave exceeding 11σ.

4. Conclusions

[46] Extensive measurements of unidirectional wavefields were carried out at a very large experimental facility, the Large Wave Channel (GWK) in Hannover, Germany. Particular attention was devoted to investigation of the effect of the initial spectral width on the statistical parameters that characterize nonlinear random water wavefields. A number of initial spectral shapes were considered, ranging from a very narrow rectangular spectrum to a moderately wide JONSWAP spectrum. The ratio of the dimensionless initial spectral widths covered the range $0.045 \leq \nu \leq 0.20$. For all spectral shapes the nonlinearity parameter was kept approximately constant, to enable decoupling of the effects of nonlinearity and of spectral width. Numerous realizations of each spectral shape with random phases of individual spectral harmonics were excited at the experimental facility by a computer-controlled wavemaker. The total duration of the records was sufficient to accumulate reliable wave statistics.

[47] The variation of all statistical parameters along the tank was found to be strongly dependent on the initial conditions. Generally speaking, the initially wider spectra remain wider than the initially narrower spectra throughout the length of the tank, so that no universal equilibrium spectral shape was

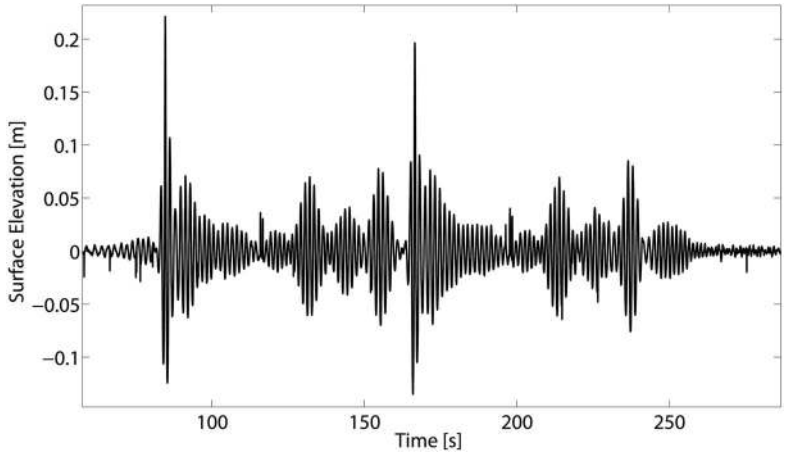

Figure 11. Record of extremely steep waves, with a height exceeding 11σ, obtained for a rectangular initial spectrum at $x = 70$ m.

attained. For each initial spectral shape a quasi-equilibrium spectral width seems to exist; it is attained at a distance of about 50 dominant wave lengths from the wavemaker.

[48] The degree of variation of various statistical parameters considered varies with the initial spectral width. These variations are the strongest for initially very narrow spectra and seem to become weaker as the width of the spectrum increases. Although the spectral shapes seem to attain quasi-equilibrium, other statistical parameters, in particular, the kurtosis and the probability distributions of wave heights, crests, and troughs, continue to vary along the whole domain of measurements. A close relation exists between the local values of the kurtosis and the behavior of the distribution tails.

[49] Freak waves appear relatively often when the initial spectrum is sufficiently narrow. Their probability for wider initial spectra is lower than that given by the Rayleigh distribution. This is in general agreement with the third-order *Tayfun and Fedele* [2007] distribution. However, for wider spectra the probability of extremely high waves seems to fall below the predictions based on both the Rayleigh and the Tayfun distributions.

[50] **Acknowledgments.** This work was supported by European Community's Sixth Framework Program through a grant to the budget of the Integrated Infrastructure Initiative HYDRALAB III within the Transnational Access Activities (contract 022441). L.S. and D.L. acknowledge the support for this study by the Israel Science Foundations under grants 964/05 and 1194/07. The work of A.S. was supported by RFBR grants 08-02-00039 and 08-05-00069 and, in part, by the European Community's Seventh Framework Programme FP7-SST-2008-RTD-1 under grant agreement 234175.

References

Annenkov, S. Y., and V. I. Shrira (2006), Direct numerical simulation of downshift and inverse cascade for water wave turbulence, *Phys. Rev. Lett.*, *96*, 204501.

Annenkov, S. Y., and V. I. Shrira (2009), Evolution of kurtosis for wind waves, *Geophys. Res. Lett.*, *36*, L13603, doi:10.1029/2009GL038613.

Dean, R. G., and R. A. Dalrymple (1991), *Water Wave Mechanics for Engineers and Scientists*, World Scientific, Singapore.

Fedele, F., Z. Cherneva, M. A. Tayfun, and C. G. Guedes Soares (2010), Nonlinear Schrodinger invariants and wave statistics, *Phys. Fluids*, *22*, 036601, doi:10.1063/1.3325585.

Goda, Y. (2000), *Random Seas and Design of Marine Structures*, World Scientific, Singapore.

Gramstad, O., and K. Trulsen (2007), Influence of crest and group length on the occurrence of freak waves, *J. Fluid Mech.*, *582*, 463–472.

Hasselmann, K. (1962), On the nonlinear energy transfer in a gravity wave spectrum. Part 1: General theory, *J. Fluid Mech.*, *12*, 481–500.

McLean, J. W. (1982), Instabilities of finite-amplitude water waves, *J. Fluid Mech.*, *114*, 315–330.

Onorato, M., A. R. Osborne, M. Serio, and L. Cavaleri (2005), Modulational instability and non- Gaussian statistics in experimental random water-wave trains, *Phys. Fluids*, *17*, 078101.

Onorato, M., A. R. Osborne, M. Serio, L. Cavaleri, C. Brandini, and C. T. Stansberg (2006), Extreme waves, modulational instability and second order theory: Wave flume experiments on irregular waves, *Eur. J. Mech. B*, *25*, 586–601.

Onorato, M., A. R. Osborne, and M. Serio (2007), On the relation between two numerical methods for the computation of random gravity waves, *Eur. J. Mech. B*, *26*, 43–48.

Onorato, M., et al. (2009), Statistical properties of mechanically generated surface gravity waves: A laboratory experiment in a three-dimensional wave basin, *J. Fluid Mech.*, *627*, 235–257.

Shemer, L., and A. Sergeeva (2009), An experimental study of spatial evolution of statistical parameters in a unidirectional narrow-banded random wavefield, *J. Geophys. Res.*, *114*, C01015, doi:10.1029/2008JC005077.

Shemer, L., K. Goulitski, and E. Kit (2007), Evolution of wide-spectrum wave groups in a tank: An experimental and numerical study, *Eur. J. Mech. B*, *26*, 193–219.

Shemer, L., A. Sergeeva, and A. Slunyaev (2010), Applicability of envelope model equations for simulation of narrow-spectrum unidirectional random field evolution: Experimental validation, *Phys. Fluids*, *22*, 011601, doi:10.1063/1.3290240.

Socquet-Juglard, H., K. Dysthe, H. Trulsen, E. Krogstad, and J. Liu (2005), Distribution of surface gravity waves during spectral changes, *J. Fluid Mech.*, *542*, 195–216.

Stiassnie, M., and L. Shemer (1987), Energy computations for coupled evolution of Class I and Class II instabilities of Stokes waves, *J. Fluid Mech.*, *174*, 299–312.

Stiassnie, M., and L. Shemer (2005), On the interaction of four water-waves, *Wave Motion*, *41*, 307–328.

Tayfun, M. A., and F. Fedele (2007), Wave height distributions and nonlinear effects, *Ocean Eng.*, *34*, 1631–1649.

Waseda, T., T. Kinishita, and H. Tamura (2009), Evolution of a random directional wave and freak wave occurrence, *J. Phys. Oceanogr.*, *39*, 621–639.

Zakharov, V. E. (1968), Stability of periodic waves of finite amplitude on the surface of deep fluid, *J. Appl. Mech. Tech. Phys.* (English transl.), *2*, 190–194.

D. Liberzon and L. Shemer, School of Mechanical Engineering, Tel-Aviv University, Tel-Aviv 69978, Israel. (Shemer@eng.tau.ac.il)

A. Sergeeva, Institute of Applied Physics, RAS, 46 Ulyanov St., 603950 Nizhny Novgorod, Russia.